Electronic Supplementary Material (ESI) for Nanoscale.

Supporting information for Evolution of high-frequency Raman modes and their doping dependence in twisted bilayer MoS_2

Rahul Debnath,[*,†,§] Indrajit Maity,[†,§] Rabindra Biswas,[‡] Varun Raghunathan,[‡] Manish Jain,[†] and Arindam Ghosh[†,¶]

Department of Physics, Indian Institute of Science, Bangalore 560012, India, Department of Electrical and Communication Engineering, Indian Institute of Science, Bangalore 560012, India, and Centre for Nano Science and Engineering, Indian Institute of Science, Bangalore 560012, India

E-mail: rahuldebnath@iisc.ac.in

[*]To whom correspondence should be addressed
[†]Department of Physics, Indian Institute of Science, Bangalore 560012, India
[‡]Department of Electrical and Communication Engineering, Indian Institute of Science, Bangalore 560012, India
[¶]Centre for Nano Science and Engineering, Indian Institute of Science, Bangalore 560012, India
[§]Contributed equally to this work

Section 1: Transport characteristics of twisted bilayer MoS_2

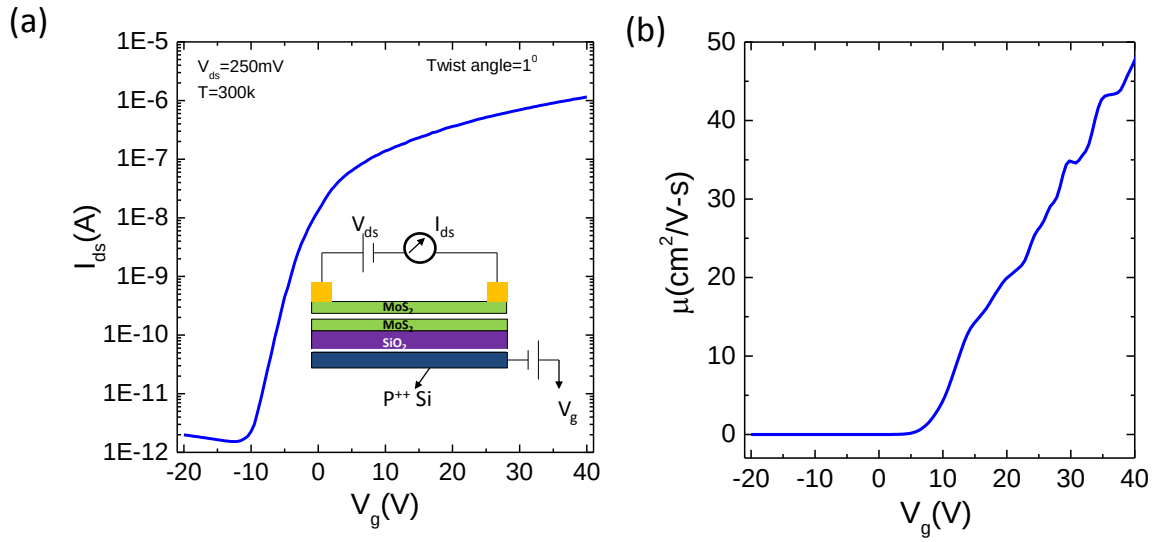

Figure S1: **Transport characteristics of twisted bilayer MoS_2.** (a) I_{ds} (source-drain current) as a function of V_g (back gate voltage) at V_{ds}=250mV (source-drain voltage). A typical schematic of the FET is presented in the inset with circuit diagram. Cr/Au(5/50nm) contacts were lithographically defined followed by thermal evaporation to create source and drain electrodes, and 285nm SiO_2 was used as the back gate. The on-off ratio of the device was $\sim 10^5$. (b) Room temperature field-effect mobility($\mu = ((1/C) \times (d\sigma/dV_g))$) of the FET at V_{ds}=250mV, where C is the gate capacitance per unit area, and $\sigma = ((L/W) \times (I/V_{ds}))$ is the linear conductivity at low bias. Here L and W are the length and width of the twisted bilayer MoS_2 channel.

Section 2: Lorentzian curve fit to the Raman spectrum

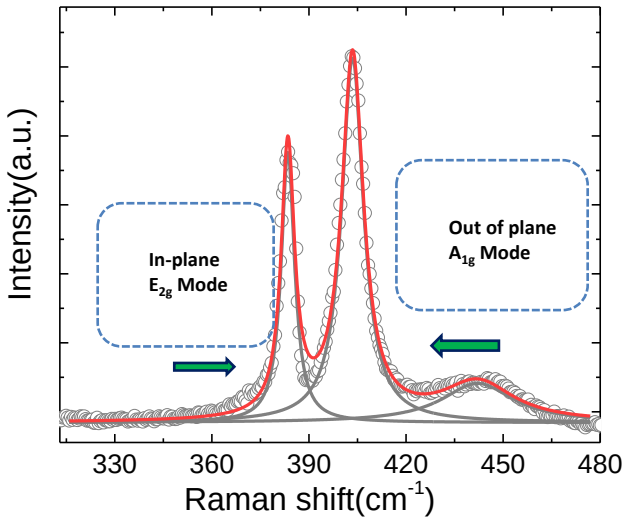

Figure S2: **Lorentzian curve fit to the Raman spectrum.** Open circles are the experimental data points, the red line is the Lorentzian fit to the total Raman spectrum, and grey lines are the Lorentzian fit to the individual peak. Line shape parameters (position of the Raman peaks, and corresponding FWHM) are obtained by using sum of three Lorentzians to the data.

Section 3: Determination of the threshold voltage (V_{Th})

.pdf

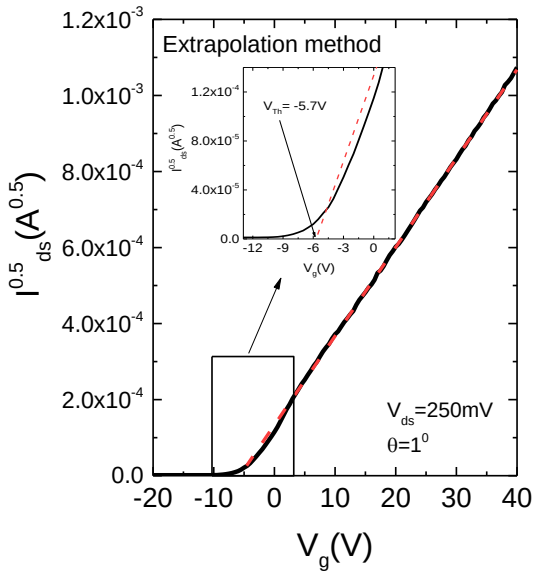

Figure S3: **Determination of the threshold voltage (V_{Th}).** Extrapolation method implemented on the measured $I^{0.5} - V_g$ characteristics of the twisted bilayer MoS2 (twist angle, $\Theta = 1°$) FET at V_{ds}=250mV. This method consist of finding the V_g axis intercept (i.e.,$I^{0.5}$=0) of the linear extrapolation of the $I^{0.5} - V_g$ curve.

Section 4: Sigmoid curve fitting for θ dependence of the peak separation

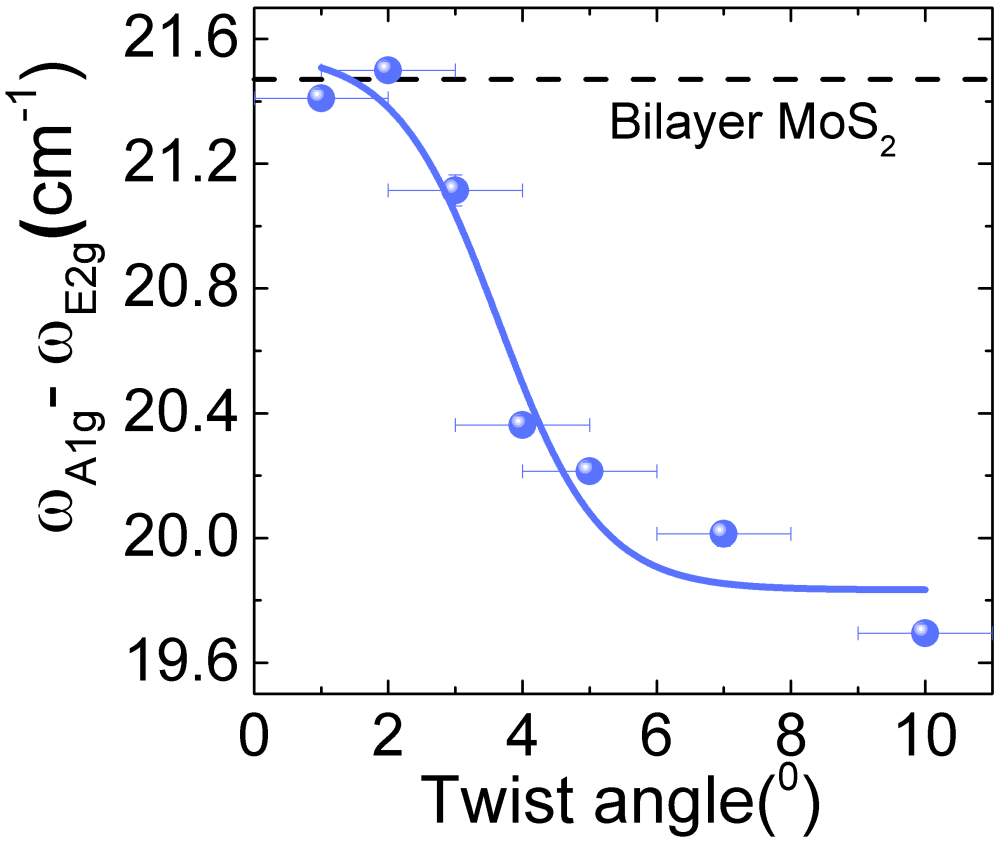

Figure S4: **Similar to the evolution of A_{1g} mode frequencies with twist angle, we fit sigmoid function for $\omega_{A_{1g}} - \omega_{E_{2g}}$ using the function : $A + (B - A)/(1 + e^{(\theta-\theta_0)/d})$. The fitted parameters $d = 0.8 \pm 0.1$, $\theta_0 = 3.6 \pm 0.1$ agree well with the parameters for the A_{1g} mode with $A = 19.8,\ B = 21.6$.**

Section 5: Calculations with local density approximation

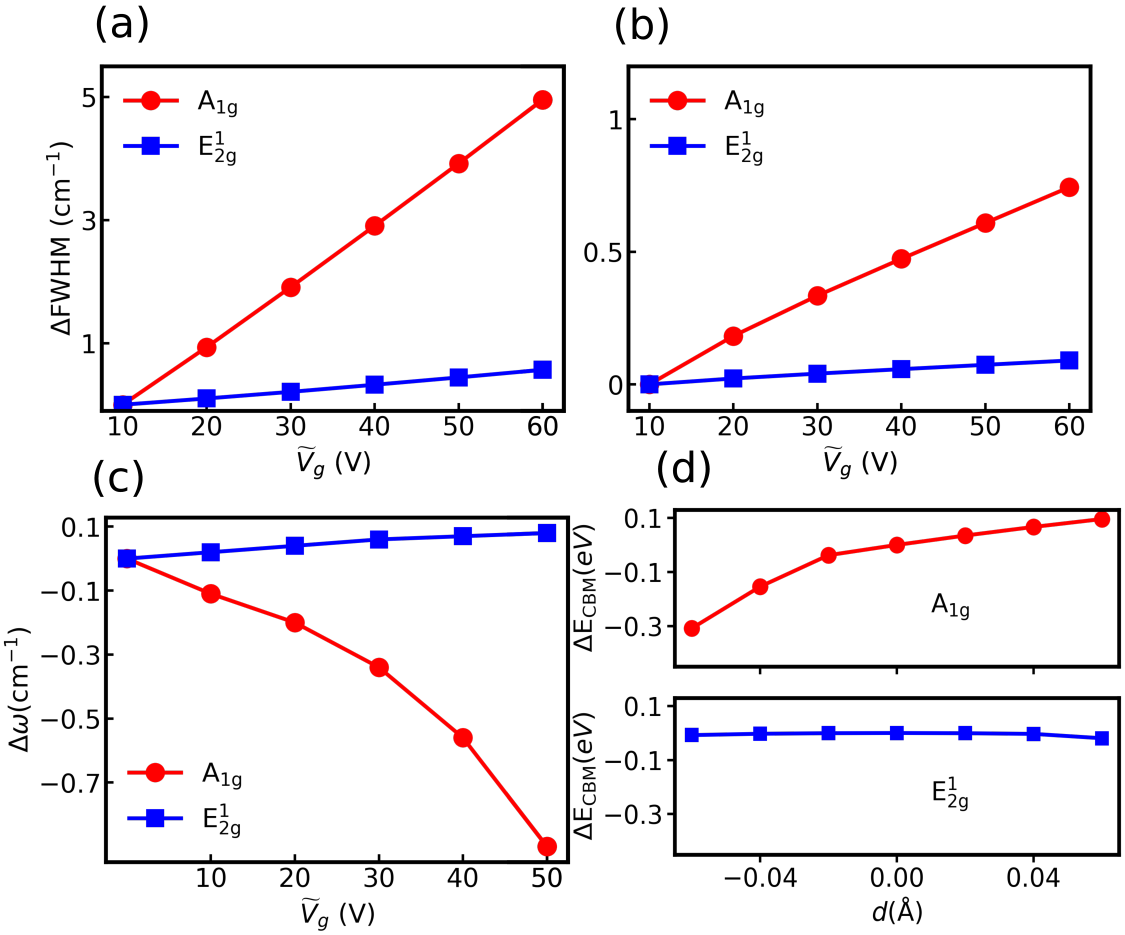

Figure S5: (a),(b) The doping dependence of linewidth of the E^1_{2g}, A_{1g} mode for single layer and bilayer MoS_2, respectively. (c) The doping dependence of the phonon mode frequencies for single layer MoS_2. (d) The change of the conduction band minimum at K point of electronic band structure due to different phonon modes with several displacement amplitude (large amplitude is used to show the difference clearly).

Depending on the exchange correlation functional used we find different CBM valleys might be occupied on electron doping for bilayer MoS_2. For instance, with LDA (GGA) the CBM in the electronic band structure for $BLMoS_2$ is at Λ (K) point. Hence, upon electron doping Λ (K) valley will be populated for LDA (GGA). In the $SLMoS_2$, upon electron doping K valley will be populated for both the exchange-correlation functional. This leads to the quantitative difference in linewidth between single and bilayer MoS_2 with LDA (whereas

almost identical behaviour with GGA). In the main text, the schematic used for different valley occupation in monolayer and bilayer MoS_2 was calculated using LDA. More accurate calculation using GW method to compute the band structures suggest that, the trends of different valley occupation captured with LDA is correct. However, the energy separation between the two valleys at Λ, K points can only be accurately captured using GW method for both mono layer and bilayer MoS_2 (which we leave for future study). The quantitative difference of the doping dependence of the phonon modes found in our experiment arise from the aforementioned valley occupation. In order to illustrate this, we compute the ratio of mono layer to bilayer electronic band curvature near the CBM for both LDA and GGA. We find the ratio with LDA to be ≈ 1.3, whereas with GGA ≈ 1. This explains the difference in linewidth found in our calculation with LDA for mono layer and bilayer MoS_2.

Section 6: Twist angle measurement using second harmonic microscopy

For the determination of armchair orientation and the twist angle measurement in a bilayer MoS_2 sample, we perform polarized second harmonic generation (P-SHG) measurement using a nonlinear microscopy setup. Here, we used a femtosecond fiber laser (Fidelity HP-10) as a fundamental excitation source operating at 1040nm, with a pulse width of 140 fs and a repetition rate of 80 MHz. The power and polarization were then controlled using a set of halfwave plate and a polarizer. Next, the MoS_2 sample was placed on a rotatory mount which was then mounted on an inverted microscope (Olympus UPLSAPO). A 20X/0.75 NA objective was used to focus the incident laser source onto the MoS2 sample. The backward SHG emission from the MoS_2 sample is then collected by the same objective and then separated from the fundamental using a dichroic mirror. After the dichroic mirror, the SHG signal is detected using a photomultiplier tube (PMT - Hamamatsu R3896). Furthermore, two bandpass (520Âś20nm) and two shortpass (890nm) filter with each having an optical density > 5 for the out-of-band signal, is mounted in front of the PMT to selectively detect the SHG signal and efficiently block any out-of-band signal. For the P-SHG measurement, we placed a wire-grid polarizer in front of the PMT. Furthermore, the incident polarization of the input laser source and the transmission axis of the wire-grid polarizer is kept fixed to horizontal with respect to the laboratory axis. The sample was then rotated in a step of 5-degree and then the two-dimensional second harmonic image for different sample orientation was obtained by scanning over the sample using a pair of galvanometric mirrors (Thorlabs GVS002).

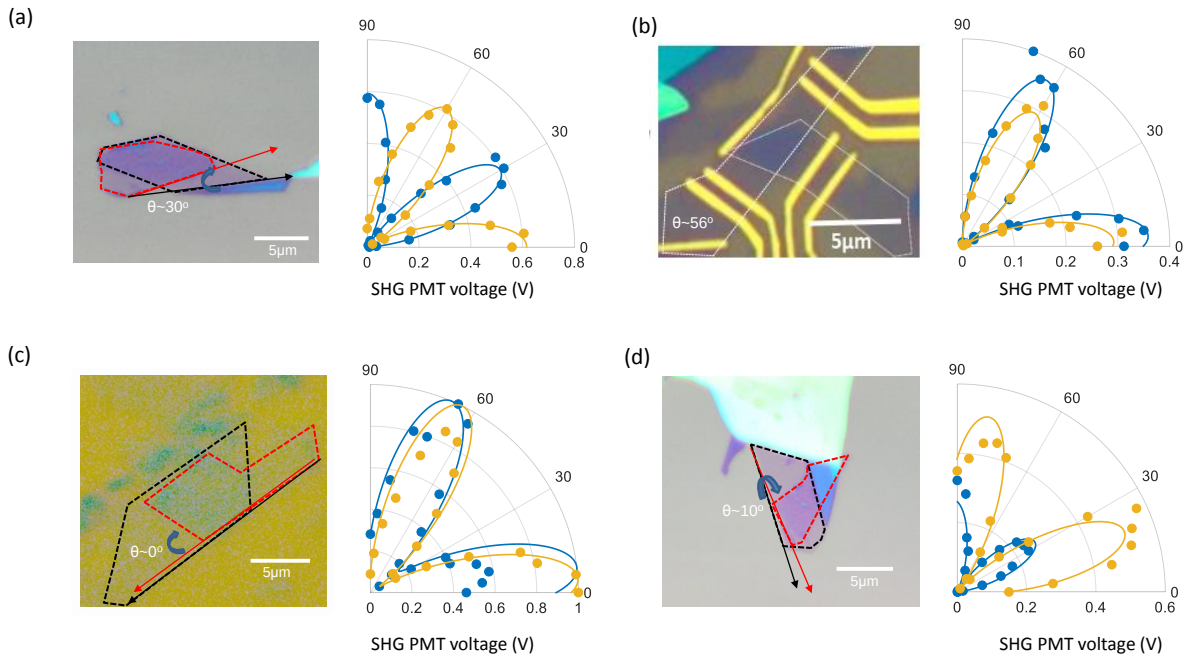

Figure S6: **Twist angle measurement using second harmonic microscopy.** (a)-(d) Optical micrograph of artificially stacked Bilayer MoS_2 and the corresponding P-SHG measurement measured from $0° \rightarrow 90°$ at various twist angle. Arrows shown in the optical image along the smooth edge of theMoS_2 correspond to zig-zag direction. Dots are the experimental data points and the solid lines are the curve fit

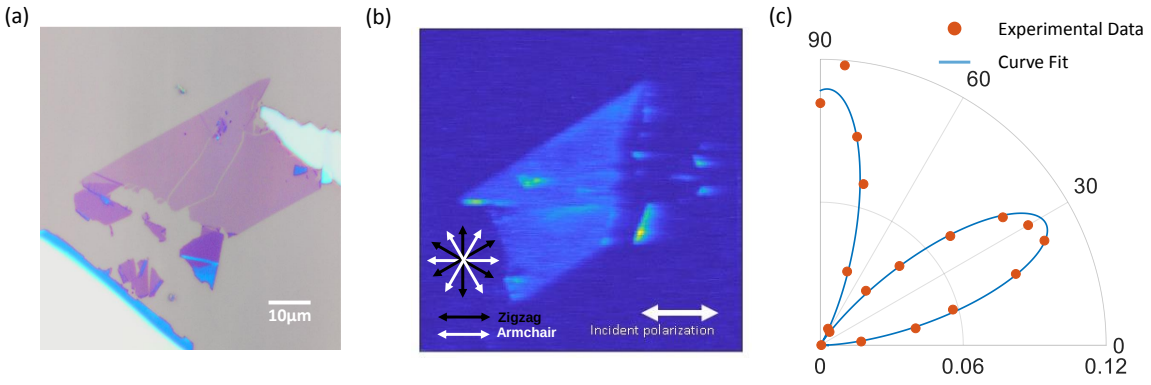

Figure S7: **Crystallographic orientation of Monolayer** MoS_2 (a)optical micrograph of Monolayer MoS_2, (b)Second harmonic microscopy image of monolayer MoS_2 and (c) the corresponding SHG measurement measured from $0° \rightarrow 90°$, which represents the straight smooth edges of MoS_2 always cleave along zig-zag direction.